



## Using injection molding and reversible bonding for easy fabrication of magnetic cell trapping and sorting devices



David Royet<sup>a,\*</sup>, Yoann Hériveaux<sup>a</sup>, Julien Marchalot<sup>a</sup>, Riccardo Scorretti<sup>a</sup>, André Dias<sup>b</sup>, Nora M. Dempsey<sup>b</sup>, Marlio Bonfim<sup>c</sup>, Pascal Simonet<sup>a</sup>, Marie Frénéa-Robin<sup>a</sup>

<sup>a</sup> Univ Lyon, ECL, UCB Lyon1, CNRS, Ampere, F-69134 Ecully, France

<sup>b</sup> Univ. Grenoble Alpes - CNRS, Inst Neel, F-38042 Grenoble, France

<sup>c</sup> Universidade Federal do Paraná, DELT, Curitiba, Brazil

### ARTICLE INFO

#### Keywords:

Cell trapping

Magnetic PDMS composites

Injection

Reversible bonding

Continuous flow sorting

### ABSTRACT

Magnetism and microfluidics are two key elements for the development of inexpensive and reliable tools dedicated to high-throughput biological analysis and providing a large panel of applications in domains ranging from fundamental biology to medical diagnostics. In this work, we introduce a simple protocol, relying on injection molding and reversible bonding for fabrication of magnetic cell trapping and sorting devices using only standard soft-lithography equipment. Magnetic strips or grids made of Polydimethylsiloxane (PDMS) doped with hard (NdFeB) or soft (carbonyl iron) magnetic powders were integrated at the bottom of whole PDMS chips. Preliminary results show the effective deviation/trapping of magnetic beads or magnetically-labeled bacteria as the sample flows through the microchannel, proving the potential of this rapid prototyping approach for easy fabrication of magnetic cell sorters.

### 1. Introduction

Microfluidic devices have been under intensive development during the past twenty years due to a number of advantages over conventional macro scale equipment, including low cost, low power consumption, small footprint, reduced sample volumes and decreased analysis times. Microfluidic technology holds great promise in the fields of life science and health care, providing new tools for single cell analysis, environmental monitoring and point-of-care diagnostics, among other applications. These fields share a common need for trapping and separation methods allowing specific and continuous isolation of cells or biomolecules from complex samples for further analysis. In this context, a large variety of microfluidic devices using different force fields (magnetic [1,2], acoustic [3], electric [4], optical [5]) or passive mechanisms allowed by careful design of the microchannel [6] have been described in the literature.

Magnetism offers many advantages for cell isolation, including great selectivity thanks to the use of superparamagnetic microbeads or nanoparticles conjugated specifically to target cells through antibody–antigen binding ([7,8]) or magnetic in situ hybridization (probe-based cell fishing [9]). Moreover, magnetic forces can attract cells over a broad spatial range and allow simultaneous manipulation of many magnetic targets, which make them suitable for high throughput cell separation. Another advantage of magnetic cell manipulation com-

pared to concurrent approaches such as dielectrophoresis is the low impact of pH, ionic strength or temperature on magnetic interactions [10].

Integration of microscale magnetic structures inside the microfluidic device enables to control the local distribution of the magnetic field while addressing the need for portability and compactness. Moreover, downscaling magnetic flux sources produces high field gradients essential for generating strong attractive forces on weakly labeled cells. Micro-electromagnets can be used to tune the field intensity but the magnetic field strength is limited to weak values due to heating issues [11]. Another widely adopted approach consists in integrating ferromagnetic microstructures (such as nickel strips [12–15] or nickel posts [16]) inside the microfluidic channel or in its vicinity [17] and using an external field to magnetize them. As a more compact alternative, permanently magnetized micropatterned hard magnetic materials were used to create the magnetic field, thereby suppressing the need for an external field source [18,19]. The above-mentioned approaches generally enable to achieve high resolution and reproducibility, but they rely on techniques which are relatively expensive, time consuming, or require expertise, like electroplating, sputtering or thermal evaporation. Micro-magnetic imprinting has been recently introduced as a new approach to fabricate composite magnetic field sources based on hard or soft magnetic micro-powders and a non magnetic matrix such as PDMS [20]. This simple and cost-effective

\* Corresponding author.

<http://dx.doi.org/10.1016/j.jmmm.2016.10.102>

Received 26 June 2016; Received in revised form 18 October 2016; Accepted 19 October 2016

Available online 21 October 2016

0304-8853/ © 2016 Elsevier B.V. All rights reserved.

process nevertheless requires the fabrication of a micro-scaled magnetic template.

Magnetic composite polymers (M-CPs) may offer a low-cost alternative to conventional microfabrication approaches [21], bringing numerous advantages such as greater accessibility to non-specialists, bio-compatibility, flexibility, ease of fabrication and ease of integration with microfluidic components thanks to compatibility with the undoped polymer.

Integration of PDMS composites in microfluidic devices is typically achieved by combining PDMS casting with the doctor blade approach [22–24], which consists in filling the recessed area of a master mold with doped PDMS before removing the excess with a soft blade. However, proper control of the final surface cleanliness is challenging and may require additional process steps involving sacrificial layers. Injection of magnetic or conductive fluids or composites into a side channel adjacent to the main microfluidic channel has been reported in several studies [25–28]. Yet, this design imposes a minimum distance between the sample channel and the magnetic material, which may result in decreased magnetic forces.

In this paper, we introduce a simple protocol to fabricate magnetic trapping and sorting devices using only standard soft-lithography equipment. The technique combining injection of M-CP with reversible bonding of PDMS enables to level the magnetic microstructures with the surface of a flat PDMS slab. First, a continuous-flow magnetic cell sorter was fabricated using simple carbonyl iron-doped PDMS strips integrated at the bottom of a whole PDMS chip with two inlets and two outlets. This classic design enables the deviation of magnetic beads or magnetically labeled cells from one flow path to another when placing a magnet under the chip [12]. Then, we demonstrate that the same fabrication process can be used to produce permanent micromagnet arrays using PDMS doped with NdFeB particles.

## 2. Materials and methods

### 2.1. Magnetic cell sorter fabrication

The fabrication of a magnetic cell sorter involves three main stages (Fig. 1):

#### a) Fabrication of a PDMS mold for magnetic polymer injection:

A network of parallel injection channels (width ranging from 50 to 200  $\mu\text{m}$ ) with a single input and single output was fabricated by replica molding using a SU-8 master mold. Briefly, a 50  $\mu\text{m}$  thick layer of negative photoresist (SU-8 2035, MicroChem) was spin-coated onto a glass slide (75 mm $\times$ 25 mm) by spinning at 500 rpm for 10 s, followed by 2000 rpm for 1 min. The coated slide was then soft baked on a hotplate at 65  $^{\circ}\text{C}$  for 2 min 30 s and baked again at 95  $^{\circ}\text{C}$  for 8 min, before being exposed for 12 s to UV light through a plastic photomask (exposure system KLOE UV-KUB, irradiance =25 mW/cm<sup>2</sup>). Post exposure baking was then performed on a hot plate at 65  $^{\circ}\text{C}$  for 1 min 30 s followed by 6 min 30 s at 95  $^{\circ}\text{C}$ . Finally, the photoresist layer was developed by immersion in Propylene glycol monomethyl ether acetate (PGMEA, Sigma-Aldrich) on a rotary shaker for 4 min. The slide was rinsed with 2-propanol, and dried under a nitrogen stream (step 1). PDMS was prepared using the Sylgard 184 Elastomer Kit (Neyco). After mixing the silicone base and the curing agent in a weight ratio of 10:1, the PDMS prepolymer was degassed in vacuum in order to remove trapped air bubbles. The prepolymer was then poured onto the SU-8 master and cured in an oven at 80  $^{\circ}\text{C}$  for 2 h (step 2). Once cured, the PDMS replica was peeled off and access holes were punched in the PDMS with a 1 mm puncher.

A thin PDMS layer (~1  $\mu\text{m}$  [29]) was deposited onto a glass slide by spin coating a 10% w/w PDMS prepolymer/heptane mixture at 4500 rpm for 1 min. The sample was then allowed to cure in an oven at 80  $^{\circ}\text{C}$  for 2 h. Afterwards, the PDMS microchannel network

and the thin PDMS layer were bound together (step 3) using air plasma treatment (Expanded Plasma Cleaner, Harrick Plasma). The closed device thereby obtained was then used as a mold for magnetic PDMS injection.

#### b) Magnetic PDMS preparation and injection:

Soft and hard micromagnet arrays were obtained using carbonyl iron and NdFeB powders (MQFP-B) provided by Sigma and Magnequench International Inc., respectively. The PDMS prepolymer was prepared following the procedure described above (10:1 wt ratio of base to curing agent) and thoroughly mixed using a metal spatula with the soft or hard powder at mass ratios of 75% and 66%, respectively. The homogenized mixture was poured into a 1 ml syringe with a flat needle at its extremity to facilitate magnetic polymer injection.

#### c) Whole device assembly:

After injection, the slide was placed on a hotplate for 2 min at 120  $^{\circ}\text{C}$  and finally baked for 2 h in an oven at 80  $^{\circ}\text{C}$ . After cooling down to room temperature, the filled PDMS mold was detached from the glass slide, thanks to the reversible bonding between the glass slide and the thin PDMS layer (step 5), and cut into pieces in order to obtain small PDMS flat slabs enclosing magnetic strips (width ranging from 50 to 200  $\mu\text{m}$  and thickness of 50  $\mu\text{m}$ ). At this stage, NdFeB composite micromagnets were permanently magnetized using a compact in-house developed pulsed magnetic field system producing a field of 6 T, uniform over a few mm. A Magneto Optic Indicator Film (MOIF) was subsequently placed above the magnetic structures to reveal the magnetized state of the doped PDMS (Figs. 4C, D). Afterwards, each PDMS block was pressed against a glass slide (strips at the bottom) and covered with freshly prepared PDMS (10:1) before curing in an oven for 2 h at 80  $^{\circ}\text{C}$  (step 6). The larger PDMS slab thereby obtained was irreversibly bonded to a PDMS cap obtained by replica molding and containing a double-Y-channel feature (width of 400  $\mu\text{m}$  and height of 50  $\mu\text{m}$ ) to form the microfluidic chip (step 7).

### 2.2. Magnetic PDMS characterization

4 mm cubes of Fe and NdFeB-doped PDMS were prepared with powder contents of 75 and 66 wt% respectively. The sample magnetic moment (A.m<sup>2</sup>) was measured as a function of applied field using an extraction magnetometer and the mass and density of each sample were determined so as to plot magnetization in T.

### 2.3. Magnetic beads

The test objects used in the trapping and sorting experiments were 10  $\mu\text{m}$ -sized magnetic micro-beads based on polystyrene (Sigma) and 1  $\mu\text{m}$ -sized streptavidin coated micro-beads (Sigma) conjugated to fluorescent Atto 550-labeled biotin.

### 2.4. Bacteria culture and labelling

Escherichia coli (DSM-No. 6897) were cultivated following the provider's recommendations (DSMZ, Germany): in Luria Bertani broth until exponential growth phase (OD=0.8). Cells were then harvested by centrifugation and labeled with 50 nm streptavidin coated superparamagnetic beads (Miltenyi Biotec), using biotinylated polyribonucleotidic probes obtained by in vitro transcription, as described by Pivetal et al. [9].

### 2.5. Microscopy

A Nikon LV150 optical microscope was used to observe magnetic bead trapping/deviation. Fluorescence imaging was also performed using a Zeiss Axio Imager equipped with a DsRed filter. SEM observations were performed using a JEOL 7401 F.

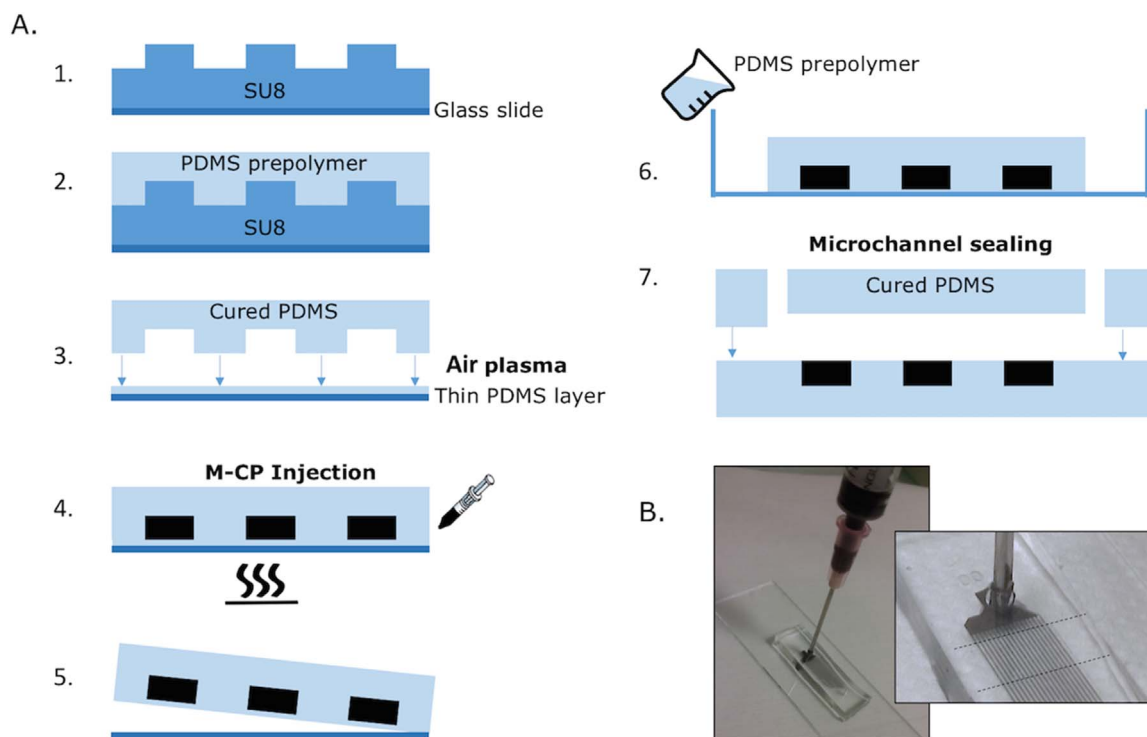


Fig. 1. A. Schematic diagram of the magnetic cell sorter fabrication process. B. Illustration of step 4: injection of the magnetic PDMS in a PDMS mold reversibly bonded to a glass slide.

2.6. Flow control setup

A NE-4000 Multi-Phaser Double Syringe pump was used to control the flow rates. For this purpose, syringe needles were connected to PTFE tubing (1/32" ID x 1/16" OD) directly inserted into the PDMS port holes of diameter 1.25 mm.

3. Results and discussion

The aim of this paper is to propose a simple and cost effective approach that can be used for the fabrication of microfluidic platforms enabling cell trapping or sorting based on magnetic interactions. The technique is based on the use of carbonyl-iron or NdFeB particles distributed in a PDMS matrix so as to obtain a composite magnetic elastomer. We demonstrate how PDMS magnetic composites (M-CP) can be micropatterned by performing M-CP injection in a microfluidic channel reversibly bonded onto a glass slide and how the magnetic microstructures thereby obtained can be integrated inside a microfluidic chip to provide a ready-to-use trapping or sorting device. In this study, two types of micropowders, namely Carbonyl Iron and NdFeB particles were mixed with PDMS to enable the fabrication of both soft and hard magnetic devices. Soft magnetic materials need to be magnetized during use, and have the advantage that the attractive force they exert on a target object can be tuned by varying the strength

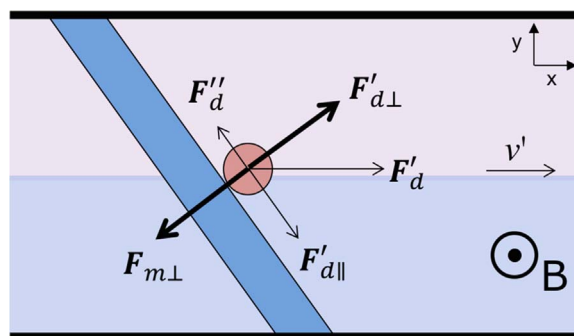


Fig. 3. Identification of forces at play. Beads are first trapped above the magnetic strip provided the in-plane magnetic force component  $F_{m\perp}$  is larger than the perpendicular component of the drag force  $F'_{d\perp}$ . Then the parallel component  $F'_{d\parallel}$  drags the beads along the strip. Note that while the bead accelerates in the strip direction, it also experiences a force opposite to its motion  $F'_{d'}$ . This force will compensate  $F'_{d\parallel}$  only when the stationary regime will be reached.

of the external magnetic field used to magnetize them. Hard magnetic materials only need to be magnetized once, and thus don't require an external field during operation, making them particularly suited for the fabrication of compact devices.

Our purpose was to integrate tilted magnetic strips made of

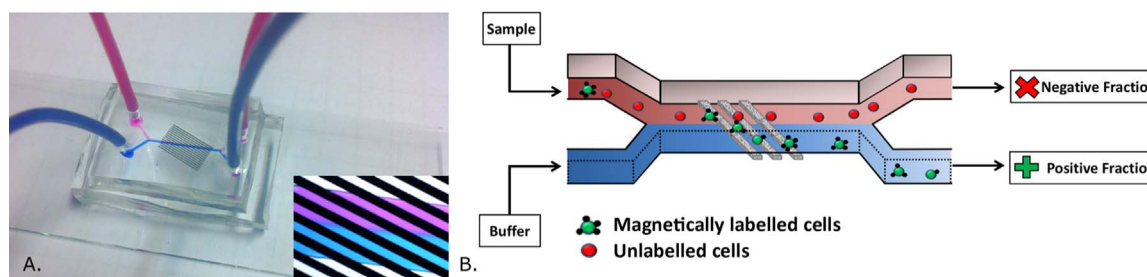
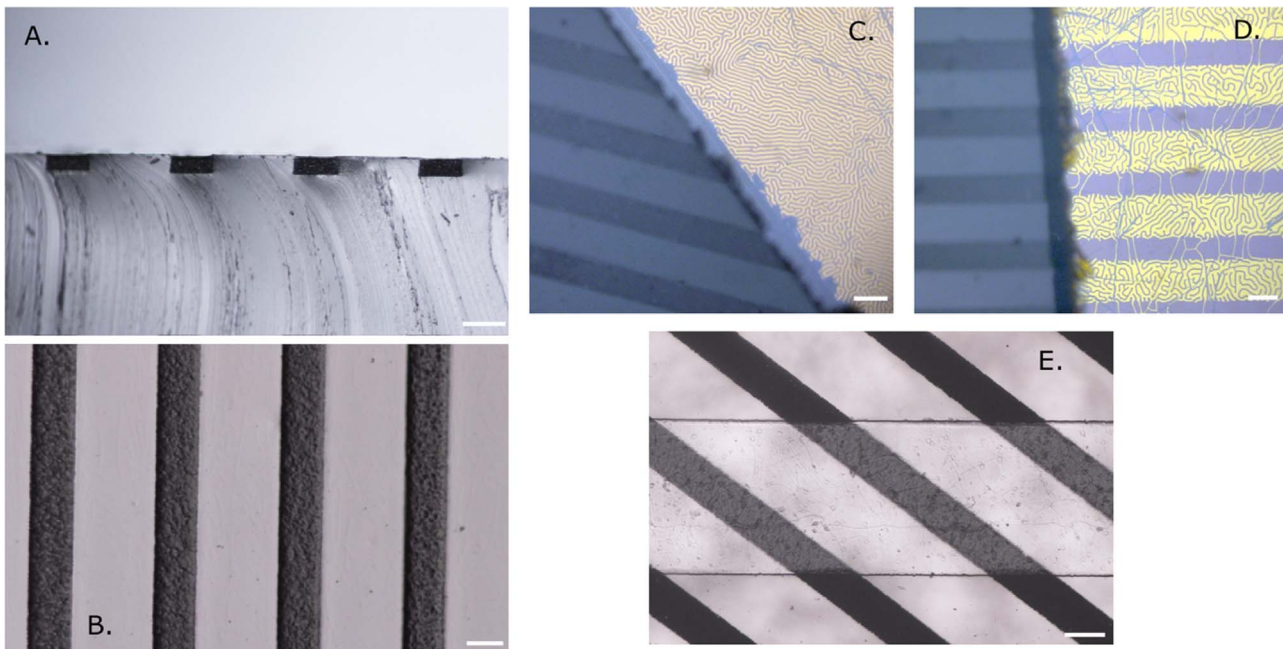


Fig. 2. A. Picture of an autonomous magnetic device integrating NdFeB strips. The inset is a zoomed image showing two laminar streams flowing side-by-side within the microfluidic channel. B. A schematic depicting the working principle of the sorting device.



**Fig. 4.** Cross view (A) and top view (B) of a PDMS flat slab with embedded soft magnetic strips. Optical images made using polarized light of a NdFeB-doped PDMS sample half covered with a Magneto-optic imaging film (MOIF): C - before magnetization; D - after magnetization. In the former we see the native magnetic domain structure of the MOIF, in the later, we see how the stray magnetic field from the underlying magnetized sample has modified the domain structure of the MOIF. E. Strips integrated at the bottom of the microfluidic chip. All scale bars are 100  $\mu\text{m}$ .

Carbonyl Iron or NdFeB-PDMS composites in a flat PDMS slab constituting the bottom of a double-Y-channel microfluidic chip, so as to obtain a continuous-flow cell sorter (Fig. 2).

Briefly, the sample containing magnetically-labeled targets is introduced via an inlet of the chip, while a bead-free buffer is introduced via the second inlet at the same flow rate. Magnetic beads are trapped and deviated along magnetic rails, thereby transferred from the sample flow path to the buffer one, which guides them to the outlet opposite to the sample inlet. Conversely, non-magnetic beads do not interact with the strips and follow the direction of fluid flow towards the facing outlet.

The main forces acting on the magnetic targets are described in Fig. 3. A spherical bead of volume  $V_b$  and magnetization  $\mathbf{M}_b$  experiences a magnetic force which can be expressed as:

$\mathbf{F}_m = \mu_0 (V_b \mathbf{M}_b \cdot \nabla) \mathbf{H}_a$ . In this equation,  $\mathbf{H}_a$  refers to the applied magnetic field at the center of the bead which is treated as an equivalent point with a magnetic dipole moment  $\mathbf{m}_{eff} = V_b \mathbf{M}_b$ . The vertical component of this force ( $\mathbf{F}_{mz}$ ) pulls the bead towards the surface of the magnetic strips.

In a carrier fluid of viscosity  $\eta$ , a bead of radius  $r$  is also submitted to fluidic Stokes' drag, which can be expressed as  $\mathbf{F}_d = 6\pi\eta r (\mathbf{v}' - \mathbf{v}'') = \mathbf{F}'_d - \mathbf{F}''_d$ , where  $\mathbf{v}'$  and  $\mathbf{v}''$  denote the respective velocities of the fluid and bead. As regards the in-plane forces applied to the bead, it should be noted that trapping of magnetic beads along the rail is possible only in the case where the magnetic force component perpendicular to the rail  $F_{m\perp}$  is larger than the perpendicular component of the drag force  $F'_{d\perp}$ . Proper guidance of the particle along the rail is then ensured by the parallel component  $F'_{d\parallel}$ .

The developed fabrication approach (Fig. 1) aims at obtaining magnetic strips leveled with the PDMS slab surface. For this purpose, we used a reversible bonding technique previously reported by our team [8,30]. The method consists here in coating the surface of a glass slide with a very thin PDMS layer (1–2  $\mu\text{m}$ ), acting as an interface layer for air plasma bonding of a microfluidic channel network, defining an injection mold for the M-CP. This technique leads to irreversible bonding between the PDMS layer and the PDMS channel, but, after injection and curing of the PDMS magnetic composite, the resulting PDMS block embedding magnetic strips can be easily pulled off the

glass slide and sealed with a PDMS cap to close the device. It should be noted that the PDMS magnetic composite had to be heated up on a hot plate directly after injection to allow rapid curing and avoid the formation of M-CP clusters during the curing process. At the end of the process, the distance separating the strips from the bottom of the separation microchannel was less than 2  $\mu\text{m}$ , which allowed magnetic interactions between the magnetic strips and the target magnetic beads to be maximized. The maximum magnetic powder / PDMS wt% that could be reached for injection was slightly lower for the NdFeB powder (66% vs 75% for the CI powder) and injection became difficult in both cases for channel widths and heights smaller than 50  $\mu\text{m}$ . The processes employed for soft and hard device fabrication were identical, except that a magnetization step was added before final sealing of the device in the case where hard material was employed (Fig. 4). With the design based on soft magnetic microstructures, a bulk permanent NdFeB magnet (remanent magnetization  $\approx 1.3$  T, energy density  $\approx 320$  kJ/m<sup>3</sup>) of size 3  $\times$  1  $\times$  0.5 cm (magnetization pointing upward) was placed perpendicularly to the channel direction, 2 mm below the magnetic strips.

Carbonyl iron particles are spherical and highly polydisperse with rather smooth surfaces, as revealed by SEM observations (Fig. 5). Their saturated magnetization is equal to 200 emu/g [31]. MQFP-B NdFeB hard powder is composed of crushed melt-spun ribbon of irregular shape and average size 5  $\mu\text{m}$ . The residual induction  $B_r$  is equal to 0.8 T, according to the datasheet. Both PDMS M-CPs were characterized using an extraction magnetometer (Fig. 6). In the case of CI-PDMS (weight ratio=3), a (mass) saturated magnetization of 161 emu/g was obtained, which is consistent with the previous finding of Li et al. [31]. The volume magnetization was also plotted in A/ m according to the applied field value, by deducing the sample volume from its mass and density (data not shown). The slope of the curve indicates an apparent susceptibility value of 1.23, which gives a relative permeability of 2.23. As regards NdFeB-PDMS, the measured remanent magnetization was found equal to  $\sim 54$  emu/g. The volume remanent magnetization deduced from sample volume measurement was found equal to  $\sim 0.2$  T.

Based on these results, the magnetic fields and field gradients obtained with soft and hard magnetic microstructures were calculated

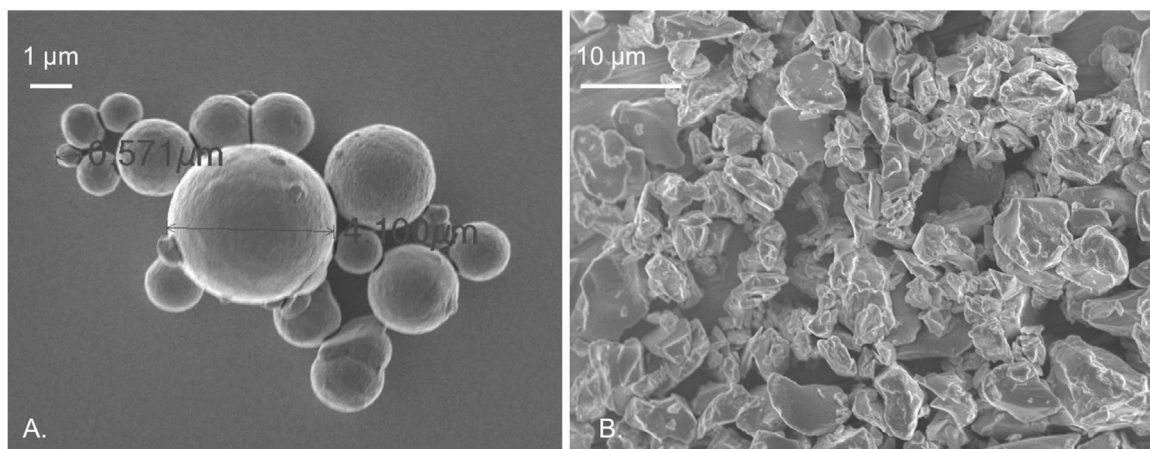


Fig. 5. SEM images of carbonyl iron particles (A) and NdFeB powder (B).

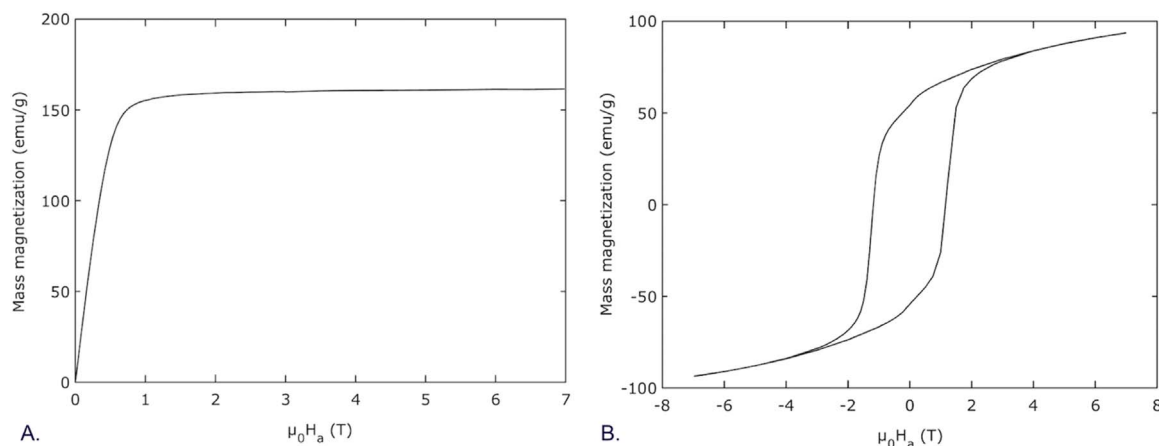


Fig. 6. A. Magnetization curve of a CI-doped PDMS sample (75 wt% carbonyl iron powder) B. Magnetization curve of a NdFeB-doped PDMS sample (66 wt% NdFeB powder).

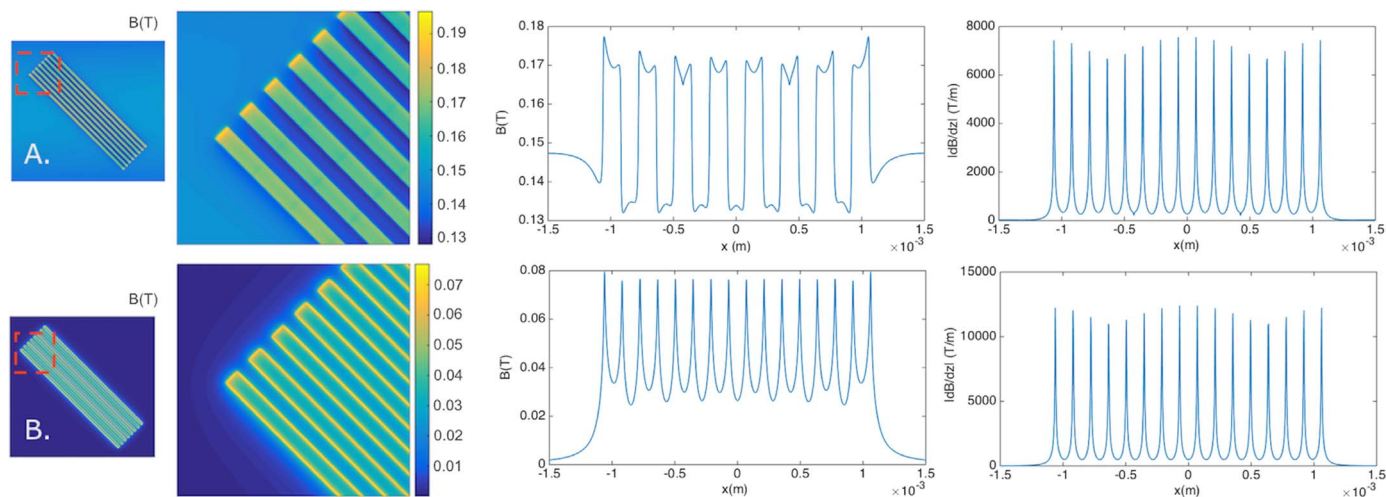
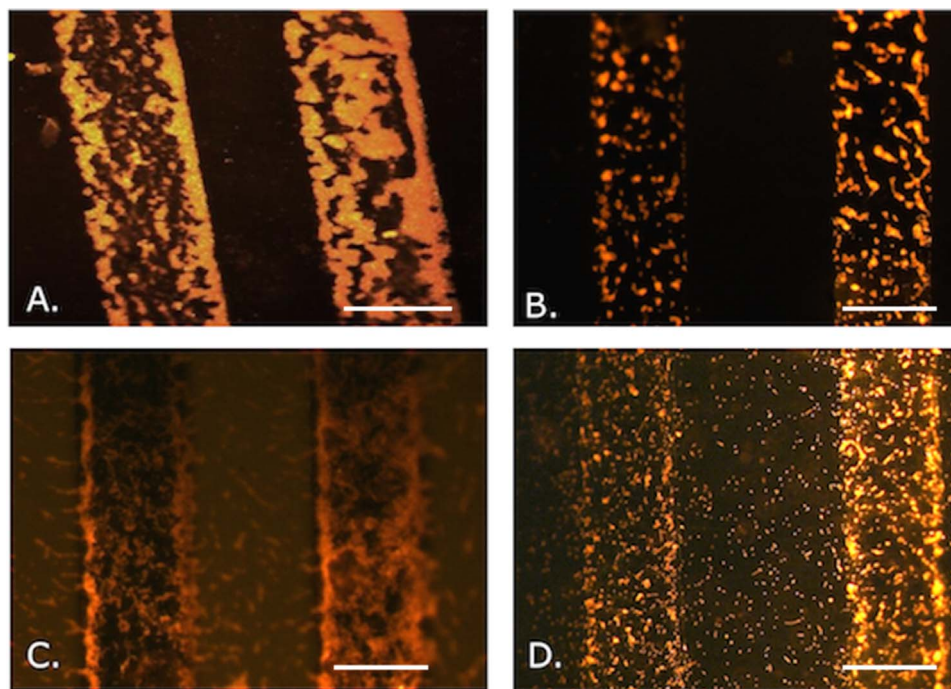


Fig. 7. Induction B and induction gradient  $dB/dz$  calculated 2 μm above the magnetic strips made with soft (A.) or (B.) hard magnetic particles. The simulations were performed for 8 strips of width 100 μm. 1-D plots were obtained for a cut line corresponding to the middle of the strips. In the case of soft magnetic strips, we observe a bias due to the stray magnetic field of the bulk magnet placed underneath ( $\approx 145$  mT).

with Matlab (Fig. 7) using a computational model described in [32]. As expected, the magnetic field values are higher in the soft material case due to the presence of the external magnet, which can be an asset as it will help to magnetize the target objects. In both cases, high field gradient values were obtained, up to  $1.3 \times 10^4$  T/m in the case of NdFeB-PDMS strips. It should be noted that such values are probably underestimated, because local inhomogeneities linked to the size and

shape of particles composing M-CP were not taken into account.

Batch trapping experiments were performed above CI-PDMS and NdFeB-PDMS strips (Fig. 8). In both cases, fluorescence observations showed that 1 μm-sized superparamagnetic beads or E.coli bacteria labeled by in-situ magnetic hybridization were successfully attracted to the strip surface. While no magnetic bead was observed between the strips, a few bacteria ( $\sim 10\%$ ) remained untrapped, which is probably



**Fig. 8.** Fluorescence imaging of 1  $\mu\text{m}$ -sized superparamagnetic beads trapped above soft (A) or hard (B) magnetic strips. Trapping of magnetically-labeled bacteria above CI (C) or NdFeB (D) strips. All scale bars are 100  $\mu\text{m}$ .

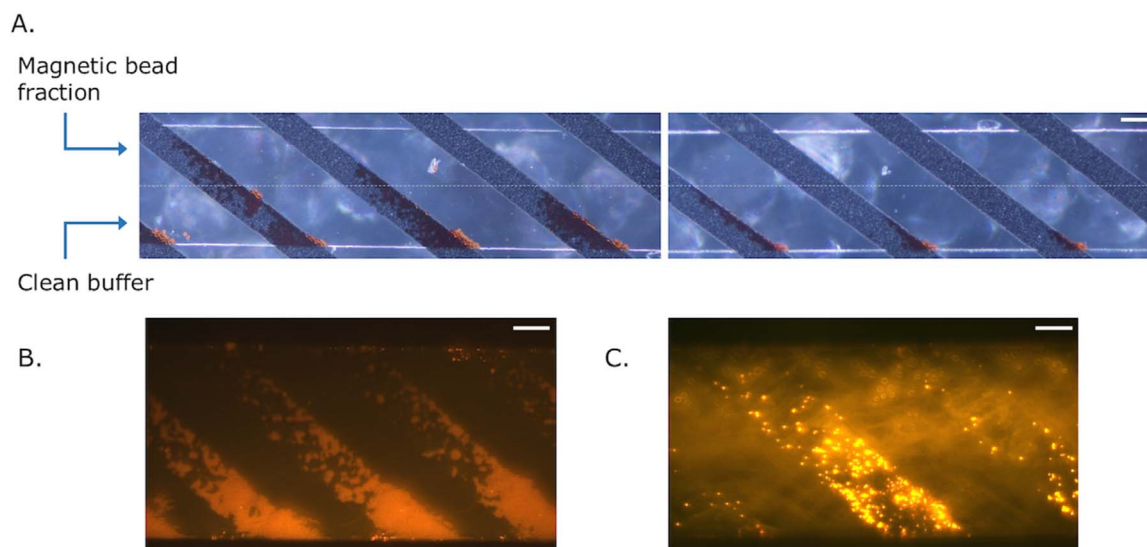


**Fig. 9.** A. Deviation of 10  $\mu\text{m}$ -sized magnetic beads from one flow path to another above an array of soft strips (dark field imaging). B. Same observations performed with 1  $\mu\text{m}$ -sized superparamagnetic beads or (C.) magnetically-labeled bacteria with NdFeB magnetic microstructures (fluorescence imaging). All scale bars are 100  $\mu\text{m}$ .

due to the fact that they were unlabeled or too weakly labeled. We also checked that unlabeled bacteria cells were randomly dispersed on the PDMS slab surface.

Continuous-flow bead trapping and deviation were also achieved with both designs, under rather high flow rates (up to 50  $\mu\text{l}/\text{min}$  when 10  $\mu\text{m}$ -sized magnetic beads were studied), as shown in Fig. 9. However, even at very high flow rates (> 500  $\mu\text{l}/\text{min}$ ), most bacteria remained trapped on the magnetic strips, probably due to adsorption problems which could be limited by bovine serum albumin pretreatment of the microsystem. As expected, the experimental set-up was more convenient with the hard magnetic version of the device, since the magnetic field sources were fully integrated in this case. In the future, the cm-sized magnet placed under the device of the soft magnetic version could be replaced by an electromagnet, so as to simplify field strength tuning.

Preliminary results also show that the proposed micro-patterning approach could be applied to the fabrication of magnetic grids using a bi-dimensional microchannel network for M-CP injection (Fig. 10A and B). Note that the stray field is maximum above holes in a magnetic surface (Fig. 10C and D). Thus in such a grid-like structure, magnetically-labeled bacteria and superparamagnetic beads are trapped at the edges of non-magnetic PDMS areas (Fig. 10E and F).

#### 4. Conclusions

We have presented a new technique to fabricate flat PDMS blocks with embedded magnetic microstructures leveled with the surface, using a combination of M-CP injection and reversible bonding. This rapid prototyping approach enables to fabricate disposable magnetic microdevices, which can be either tunable or autonomous using soft or

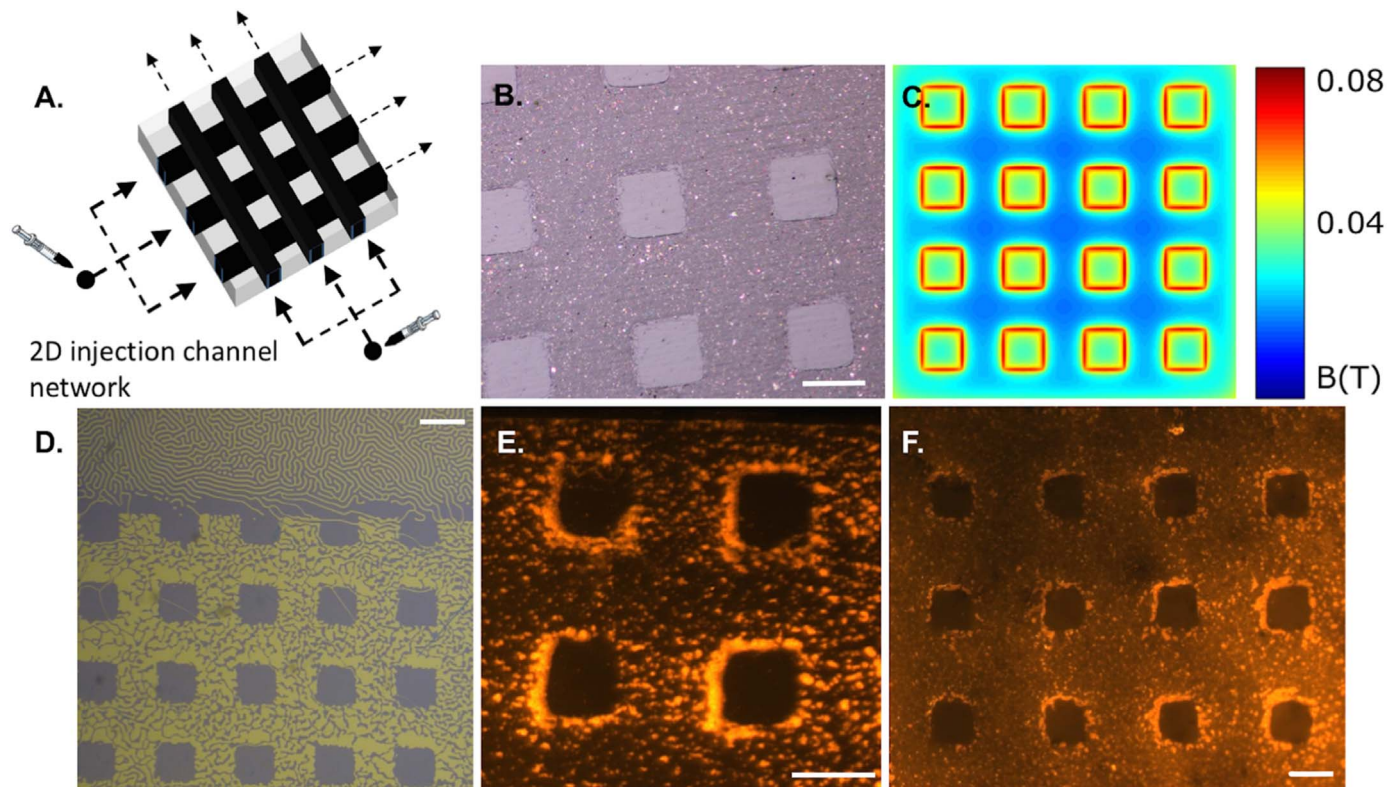


**Fig. 10.** A. Illustration of the potential of the technique for the fabrication of magnetic grids. B. Picture of the magnetic grid obtained after 2D injection above a grid of hard magnetic particles. C. Induction  $B$  (T) calculated 2  $\mu\text{m}$  above the grid. D. Magneto-optic imaging of a grid obtained using the hard magnetic powder. Magnetically-labeled bacteria (E.) and 1  $\mu\text{m}$ -sized superparamagnetic beads (F.) trapped around square zones corresponding to undoped PDMS areas. Scale bars: 100  $\mu\text{m}$ .

hard magnetic material, respectively. We have demonstrated bead trapping and deviation under continuous flow, which could be useful for biological applications involving medium exchange or cell sorting. Future work will consist in applying this approach to the isolation of specific bacterial cells from a complex sample using magnetic in-situ hybridization [9]. Other designs including 2D magnetic arrays will be further investigated and the magnetic field simulations will also be supplemented by on-going analysis of fluid-bead transport so as to obtain bead trajectories.

### Acknowledgements

The authors gratefully acknowledge financial support from the LabEx iMUST – Université de Lyon, Institute for Multiscale Sciences & Technologie (ANR-10-LABX-0064/ANR-11-IDEX-0007) and from French Ministry of Education and Research. They also wish to thank Pierre Cremillieu at INL (Nanolyon platform) for his technical support regarding SEM imaging.

### References

- [1] N. Pamme, C. Wilhelm, Continuous sorting of magnetic cells via on-chip free-flow magnetophoresis, *Lab Chip* 6 (2006) 974–980. <http://dx.doi.org/10.1039/b604542a>.
- [2] K. Hoshino, Y.-Y. Huang, N. Lane, M. Huebschman, J.W. Uhr, E.P. Frenkel, X. Zhang, Microchip-based immunomagnetic detection of circulating tumor cell, *Lab Chip* 11 (2011) 3449–3457. <http://dx.doi.org/10.1039/b000000x/Hoshino>.
- [3] S.H. Cho, C.H. Chen, F.S. Tsai, J.M. Godin, Y.-H. Lo, Human mammalian cell sorting using a highly integrated micro-fabricated fluorescence-activated cell sorter ( $\mu\text{FACS}$ ), *Lab Chip* 10 (2010) 1567–1573. <http://dx.doi.org/10.1039/c000136h.Human>.
- [4] K. Takahashi, A. Hattori, I. Suzuki, T. Ichiki, K. Yasuda, Microscopic image processing, *J. Nanobiotechnol.* 8 (2004) 1–8. <http://dx.doi.org/10.1186/1477-3155-2-5>.
- [5] J. Enger, M. Goksör, K. Ramser, P. Hagberg, D. Hanstorp, Optical tweezers applied to a microfluidic system, *Lab Chip* 4 (2004) 196–200. <http://dx.doi.org/10.1039/b307960k>.
- [6] D.R. Gossett, W.M. Weaver, A.J. MacH, S.C. Hur, H.T.K. Tse, W. Lee, H. Amini, D. Di Carlo, Label-free cell separation and sorting in microfluidic systems, *Anal. Bioanal. Chem.* 397 (2010) 3249–3267. <http://dx.doi.org/10.1007/s00216-010-3721-9>.
- [7] T.P. Forbes, S.P. Forry, Microfluidic magnetophoretic separations of immunomagnetically labeled rare mammalian cells, *Lab Chip* 12 (2012) 1471–1479. <http://dx.doi.org/10.1039/c2lc40113d>.
- [8] O. Osman, S. Toru, F. Dumas-Bouchiat, N.M. Dempsey, N. Haddour, L.-F. Zanini, F. Buret, G. Reyne, M. Frénéa-Robin, Microfluidic immunomagnetic cell separation using integrated permanent micromagnets, *Biomicrofluidics* 7 (2013) 054115. <http://dx.doi.org/10.1063/1.4825395>.
- [9] J. Pivetal, S. Toru, M. Frenea-Robin, N. Haddour, S. Cecillon, N.M. Dempsey, F. Dumas-Bouchiat, P. Simonet, Selective isolation of bacterial cells within a microfluidic device using magnetic probe-based cell fishing, *Sens. Actuators B Chem.* 195 (2014) 581–589. <http://dx.doi.org/10.1016/j.snb.2014.01.004>.
- [10] N. Pamme, Magnetism and microfluidics, *Lab Chip* 6 (2006) 24–38. <http://dx.doi.org/10.1039/b513005k>.
- [11] Q. Ramadan, D.P. Poenar, C. Yu, Customized trapping of magnetic particles, *Microfluid. Nanofluid.* 6 (2009) 53–62. <http://dx.doi.org/10.1007/s10404-008-0296-2>.
- [12] D.W. Inglis, R. Riehn, R.H. Austin, J.C. Sturm, Continuous Microfluidic immunomagnetic cell separation, *Appl. Phys. Lett.* 85 (2004) 5093–5095. <http://dx.doi.org/10.1063/1.1823015>.
- [13] J.D. Adams, U. Kim, H.T. Soh, Multitarget magnetic activated cell sorter, *Proc. Natl. Acad. Sci. USA* 105 (2008) 18165–18170. <http://dx.doi.org/10.1073/pnas.0809795105>.
- [14] J. Jung, K.H. Han, Lateral-driven continuous magnetophoretic separation of blood cells, *Appl. Phys. Lett.* 93 (2008) 1–4. <http://dx.doi.org/10.1063/1.3036898>.
- [15] P.L. Guo, M. Tang, S.L. Hong, X. Yu, D.W. Pang, Z.L. Zhang, Combination of dynamic magnetophoretic separation and stationary magnetic trap for highly sensitive and selective detection of Salmonella typhimurium in complex matrix, *Biosens. Bioelectron.* 74 (2015) 628–636. <http://dx.doi.org/10.1016/j.bios.2015.07.019>.
- [16] T. Deng, M. Prentiss, G.M. Whitesides, Fabrication of magnetic microfiltration systems using soft lithography, *Appl. Phys. Lett.* 80 (2002) 461. <http://dx.doi.org/10.1063/1.1436282>.
- [17] N. Xia, T.P. Hunt, B.T. Mayers, E. Alsborg, G.M. Whitesides, R.M. Westervelt, D.E. Ingber, Combined microfluidic-micromagnetic separation of living cells in continuous flow, *Biomed. Micro.* 8 (2006) 299–308. <http://dx.doi.org/10.1007/s10544-006-0033-0>.
- [18] F. Dumas-Bouchiat, L.F. Zanini, M. Kustov, N.M. Dempsey, R. Grechishkin, K. Hasselbach, J.C. Orlianges, C. Champeaux, a. Catherinot, D. Givord, Thermomagnetically patterned micromagnets, *Appl. Phys. Lett.* 96 (2010) 1–4. <http://dx.doi.org/10.1063/1.3341190>.

- [19] L.F. Zanini, N.M. Dempsey, D. Givord, G. Reyne, F. Dumas-Bouchiat, Autonomous micro-magnet based systems for highly efficient magnetic separation, *Appl. Phys. Lett.* 99 (2011) 2011–2014. <http://dx.doi.org/10.1063/1.3664092>.
- [20] N.M. Dempsey, D. Le Roy, H. Marelli-Mathevon, G. Shaw, A. Dias, R.B.G. Kramer, L. Viet Cuong, M. Kustov, L.F. Zanini, C. Villard, K. Hasselbach, C. Tomba, F. Dumas-Bouchiat, Micro-magnetic imprinting of high field gradient magnetic flux sources, *Appl. Phys. Lett.* 104 (2014) 14–19. <http://dx.doi.org/10.1063/1.4886375>.
- [21] B.L. Gray, A review of magnetic composite polymers applied to microfluidic devices, *J. Electrochem. Soc.* 161 (2014) B3173–B3183. <http://dx.doi.org/10.1149/2.023402jes>.
- [22] B. Teste, N. Jamond, D. Ferraro, J.-L. Viovy, L. Malaquin, Selective handling of droplets in a microfluidic device using magnetic rails, *Microfluid. Nanofluid.* 19 (2015) 141–153. <http://dx.doi.org/10.1007/s10404-015-1556-6>.
- [23] A.-L. Deman, M. Brun, M. Quatresous, J.-F. Chateaux, M. Frenea-Robin, N. Haddour, V. Semet, R. Ferrigno, Characterization of C-PDMS electrodes for electrokinetic applications in microfluidic systems, *J. Micromech. Microeng.* 21 (2011) 1–8. <http://dx.doi.org/10.1088/0960-1317/21/9/095013>.
- [24] M. Faivre, R. Gelszinnis, J. Degouttes, N. Terrier, C. Rivière, R. Ferrigno, A.-L. Deman, Magnetophoretic manipulation in microsystem using carbonyl iron-polydimethylsiloxane microstructures, *Biomicrofluidics* 8 (2014) 054103. <http://dx.doi.org/10.1063/1.4894497>.
- [25] R. Zhou, C. Wang, Microfluidic separation of magnetic particles with soft magnetic microstructures, *Microfluid. Nanofluidics* (2016) 1–11. <http://dx.doi.org/10.1007/s10404-016-1714-5>.
- [26] A.C. Siegel, S.S. Shevkopylas, D.B. Weibel, D.A. Bruzewicz, A.W. Martinez, G.M. Whitesides, Cofabrication of electromagnets and microfluidic systems in poly(dimethylsiloxane), *Angew. Chem. - Int. Ed.* 45 (2006) 6877–6882. <http://dx.doi.org/10.1002/anie.200602273>.
- [27] J.J. Agresti, E. Antipov, A.R. Abate, K. Ahn, A.C. Rowat, J.-C.J.-C. Baret, M. Marquez, A.M. Klibanov, A.D. Griffiths, D. a. Weitz, Ultrahigh-throughput screening in drop-based microfluidics for directed evolution, *Proc. Natl. Acad. Sci.* 107 (2010) 4004–4009. <http://dx.doi.org/10.1073/pnas.0910781107>.
- [28] Y. “Adam” Lin, T.-S. Wong, U. Bhardwaj, J.-M. Chen, E. McCabe, C.-M. Ho, Formation of high electromagnetic gradients through a particle-based microfluidic approach, *J. Micromech. Microeng.* 17 (2007) 1299–1306. <http://dx.doi.org/10.1088/0960-1317/17/7/012>.
- [29] S. Menad, A. El-Gaddar, N. Haddour, S. Toru, M. Brun, F. Buret, M. Frenea-Robin, From bipolar to quadrupolar electrode structures: an application of bond-detach lithography for dielectrophoretic particle assembly, *Langmuir* 30 (2014) 5686–5693. <http://dx.doi.org/10.1021/la5005193>.
- [30] C. Vézy, N. Haddour, N.M. Dempsey, F. Dumas-Bouchiat, M. Frenea-Robin, Simple method for reversible bonding of a polydimethylsiloxane microchannel to a variety of substrates, *Micro Nano Lett.* 6 (2011) 871. <http://dx.doi.org/10.1049/mnl.2011.0492>.
- [31] J. Li, M. Zhang, L. Wang, Design and fabrication of microfluidic mixer from carbonyl iron – PDMS composite membrane, *Microfluid. Nanofluidics* 10 (2011) 919–925. <http://dx.doi.org/10.1007/s10404-010-0712-2>.
- [32] S.A. Khashan, E.P. Furlani, Coupled particle–fluid transport and magnetic separation in microfluidic systems with passive magnetic functionality, *J. Phys. D: Appl. Phys.* 46 (2013) 125002. <http://dx.doi.org/10.1088/0022-3727/46/12/125002>.